EasyChair Preprint

№ 4596

Numerical Simulation for Transformer Winding Thermal Analysis Between Detailed Winding and Simplified Winding Models

Zulkifli Ibrahim, Mohd Zainal Abidin Ab. Kadir, Norhafiz Azis, Jasronita Jasni and Muhammad Hakirin Roslan

November 18, 2020

Zulkifli Ibrahim[1,2*], Mohd Zainal Abidin Ab. Kadir[2,3], Norhafiz Azis[2], Jasronita Jasni[2], Muhammad Hakirin Roslan[4]

J. Electrical Systems x-x (xxxx): xxx-xxx

Regular paper

Numerical simulation for transformer winding thermal analysis between detailed winding and simplified winding models

Ability to predict and measure the hot-spot temperature is undoubtfully a key in developing thermal quality of transformer design. The hot-spot temperature is a very important parameter in transformer load management and a significant parameter to determine the thermal performances and loss of life prediction. Thermal-hydraulic network model (THNM) and CFD are very useful methods to model the temperature distribution inside the transformer winding. Performance-wise the CFD is far more advanced in providing detail study, but there are drawbacks such as complexity, very time consuming and very costly. This paper presents a two-dimensional (2D) axis symmetric CFD winding simplified model for both small distribution and medium power transformers. They are developed in favor to reduce model's geometric complexity. The cooling effects of natural oil convection are observed on both oil flow and thermal distributions. Results show the SM is not recommended for detailed thermal and flow studies on the medium power transformer (disc winding), but it's a good approach for small distribution transformer (layer winding). However, the SM is recommended during the early design stage for both transformers due to small variation in average winding temperature.

Keywords: hot-spot temperature; hot-spot location; Computational Fluid Dynamic (CFD); natural oil convection; transformer; disc winding; layer winding

1. Introduction

Transformer is one of the complex electrical devices in a power system network in terms of construction as well as its operating behavior and has the efficiency of around 98 percent [1]. To best describe the physics operation of a transformer is the Faraday's law of induction which was discovered in 1831[2]. Today's thermal management of power transformers is getting complex due to the existence of the new concept of power system networks. For instance, renewable energy, distributed generation system and direct-current charging station system networks. These networks involve power electronics converter by which it will contribute to increasing the harmonic component in the system. Subsequently, it will increase the normal operating temperature of the transformer[3],[4]. As such these factors decrease the limitation of transformer loading capacity [5].

The transformer life expectancy is the relative aging rate of oil-impregnated insulation paper where the relative aging rate is a time function of temperature [6]. The temperature rise inside the transformer is proportional to the heat developed by the winding losses. This heat must be cooled by a specific cooling mechanism. Most of the transformer is cooled by the natural convection of oil circulates between windings and active-parts through cooling ducts. The flow of oil inside the transformer is influenced by the buoyancy effects due to the changes in oil viscosity. The heated oil then flows between radiators for the external cooling mechanism either by air natural or air forced convection.

Cooling design always a challenge to transformer designers, selection of type and number of radiators are crucial to avoid overheating at any parts of the transformer. At the beginning of design work, the designer must come out with a quotation design within a limited time, thus a fast and reliable data during this stage are very important. In quotation design, detail components and its quantity must be at the minimum as possible so that the requested transformer can be quoted at a reasonable/winnable price. At this stage, designer relies on one-dimensional in-house THNM and analytical computation. Even though the THNM and analytical computation can provide reliable data especially on average design

* Corresponding author: Zulkifli Ibrahim, Faculty of Electrical and Electronic Engineering Technology, Universiti Teknikal Malaysia Melaka, Durian Tunggal 76100, Malaysia; E-mail: zulkifliibrahim@utem.edu.my

[1] Faculty of Electrical and Electronic Engineering Technology, Universiti Teknikal Malaysia Melaka, Durian Tunggal 76100, Malaysia

[2] Centre for Electromagnetic and Lightning Protection Research (CELP), Advanced Lightning and Power Energy Research (ALPER), Universiti Putra Malaysia, 43400 Serdang, Selangor, Malaysia

[3] Institute of Power Engineering (IPE), Universiti Tenaga Nasional, 43000 Kajang, Malaysia

[4] Faculty of Engineering, Universiti Pertahanan Nasional Malaysia, Kem Sg Besi 57000, Malaysia

temperature, but they are unable to provide details thermal distribution. Consequently, it will be very difficult for designers to make a good decision on cooling arrangements.

Due to this scenario, a CFD based computer-aided tool is the best method for solving cooling design problem [7]. The CFD is one of the powerful computer-aided tools to perform a simulation of electromagnetic, heat transfer and flow problems. The CFD become very popular these days due to its ability to perform a detailed study on the transformer winding. However, without thorough software understanding, the CFD can become very complex, time-consuming and very costly [8]. In addition, most of the manufacturers use the CFD techniques at the final stage of the design process and it is not feasible for routine design work due to high computational requirement.

To date, the CFD is widely used in modern transformer design and analysis due to its ability to perform detailed transformer study. Many scientific works of literature provide in-depth CFD based detailed thermal study on transformer winding. Gong et al.[9] presented the implementation of three-dimensional (3D) magneto-fluid-thermal coupled to calculate temperature distribution within windings, thus provides optimization method of the cooling design. Campelo et al. [10] performed comparisons of mass flow rate and disc temperature between in-house developed thermal models (namely THNM1 and THNM2) and a 3D CFD model. In his study, the CFD model was able to spot the hot-spot location while none in the THNMs. The oil leakage effects study was performed by Paramane et al. [11] where the winding and fluid thermal performances were analyzed based on the percentage of oil leakage due to the imperfection of washer fixation. Guan et al. [12] investigated the heat transfer in distribution transformer filled with nanofluid, where the distribution of nanoparticles and electrophoresis were considered in the CFD simulation. On top of that, the CFD is also used to calibrate the in-house THNM equations [11],[13]. Modelling the transformer winding is very important to correctly estimates the hot-spot temperature and its location. This estimated hot-spot value is beneficial in estimating the lifespan of the transformer, thus it is very useful for further action such as planning for replacement or maintenance.

The objective of this paper is to compare and analyze the CFD model for both simplified and detailed windings. In this paper, investigations on thermal distributions inside windings are presented in 2D CFD approximation. Comparisons between DM and SM were graphically well explained. Finally, recommendation on the suitability of SM to be used during the early design stage i.e. quotation design. This paper investigates two different oil-immersed three-phase transformers namely 1000kVA 11/0.415kV and 30MVA 33/11kV. These two transformers are selected due to different winding constructions. The 1000kVA uses copper-foil as a conductor with layer type of winding while the 30MVA uses rectangular conductor with helical/disc winding type.

2. Model descriptions

2.1. Transformer fluid and solid materials

All transformers in this study use the following properties for oil and solid materials. The physical properties of transformer oil are modeled to vary with temperature and constant with pressure. They are expressed as follow [8],

$$\rho_f = 1098.72 - 0.712\ T_f \tag{1}$$

$$k_f = 0.1509 - 7.101\times10^{-5}\ T_f \tag{2}$$

$$C_{pf} = 807.163 + 3.58\ T_f \tag{3}$$

$$\mu = 0.08467 - 0.0004\ T_f + 5\times10^{-7}\ T_f^2 \tag{4}$$

where ρ_f is the fluid density, k_f denotes as thermal conductivity, C_p is the specific heat capacity at constant pressure, μ stands for dynamic viscosity and T_f is the temperature of the oil. The solid materials are considered isotropic and independent to the temperature and pressure. The copper conductor has 8933 kg/m^3, 385 J/(K·kg) and 401W/(K·m) for (ρ_c) density, specific heat capacity (C_{pc}) and (k_c) thermal conductivity respectively. The (ρ_p) density, (C_{pp}) specific heat capacity and (k_p) thermal conductivity for the insulation paper are 930 kg/m3, 1340 J/(K·kg) and 0.19 W/(K·m) respectively.

2.2. 1000kVA 11/0.433kV small distribution transformer

This hermetically-sealed type transformer serves at distribution level having a single type of cooling mode i.e oil-natural-air-natural (ONAN). The 0.415 volts of LV winding is made up by 16 turns of 430mm x1.3mm copper foil. Each turn is separated by the 0.07mm thick of diamond-dotted insulation paper. The axial cooling channel is developed after the 8th turn by inserting 4.5mm corrugated pressboard. There are two sections of LV winding namely S1 for inner-side and S2 for outer-side of winding. The LV winding is designed in such a way that the oil flow naturally enters the winding from the bottom of the tank and leaves the winding at the top. Details of the LV winding configuration are shown in Figure 1. At full load, this transformer carries 1333.33 A per phase on the LV side making its current density equals to 2.38 A/mm^2. The winding loss is computed by

$$P_{dc}= J^2 \cdot \frac{\sigma \cdot m}{\rho_c} \tag{5}$$

where P_{dc} t is the resistive loss, J represents the current density, σ stands for conductivity, m is the length and ρ_c is the density of conductor. The axial eddy loss, $P_{e,a}$ is expressed by

$$P_{e,a}= k_{e,h} \frac{f^2 \cdot B_a^2}{\rho_c} \tag{6}$$

and the radial eddy loss $P_{e,r}$ can be expressed as

$$P_{e,r}= k_{e,w} \frac{f^2 \cdot B_r^2}{\rho_c} \tag{7}$$

where $k_{e,h}$ and $k_{e,w}$ are the conductor height and width respectively, f is the frequency; B_a and B_r are the axial and radial magnetic flux density respectively. These give the LV total losses per phase equals to 1036 watts.

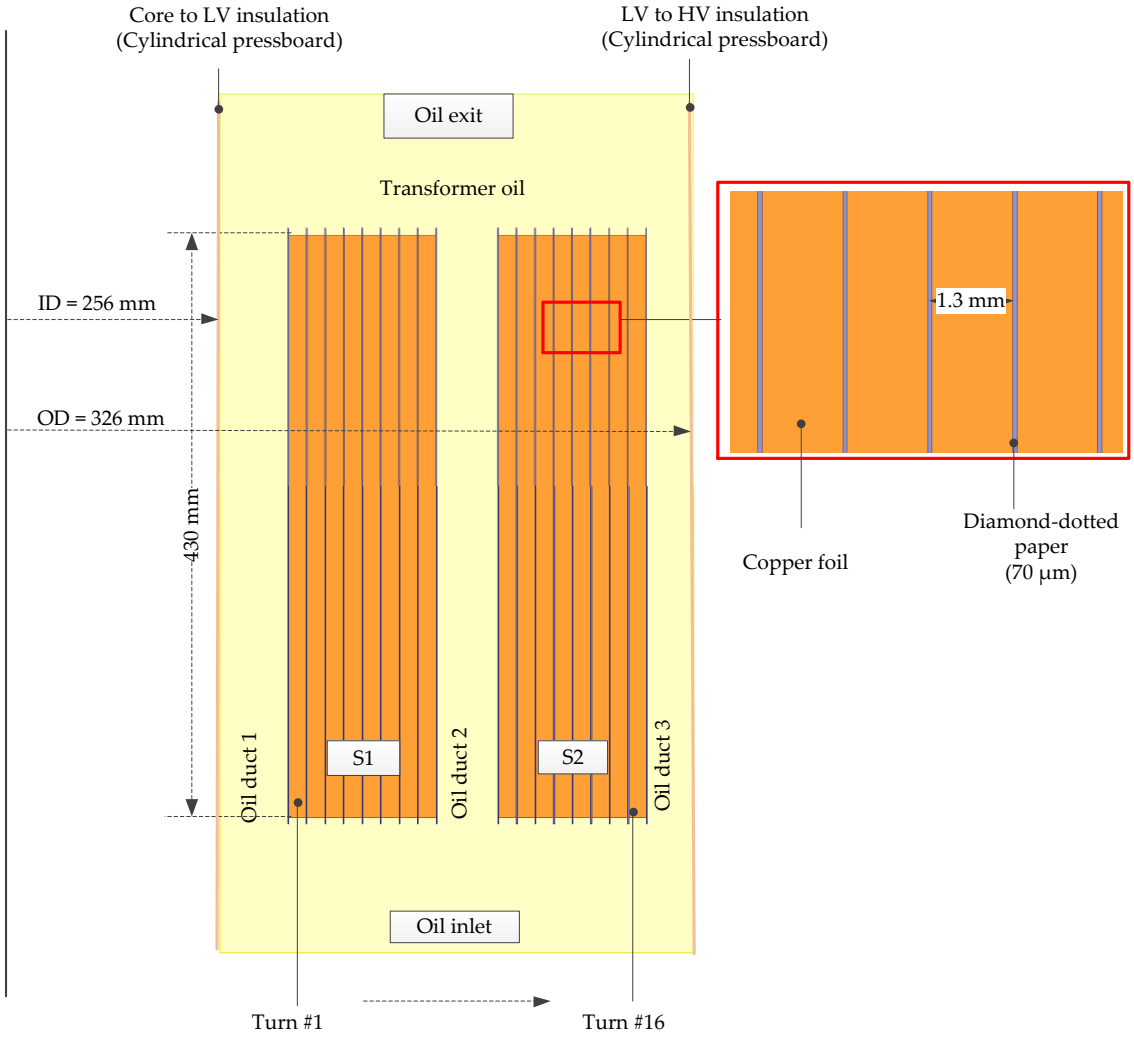

Figure 1. 2D axis-symmetric of 0.433kV detailed LV winding model with a close-up view of winding components.

2.3. 30MVA 33/11kV medium power transformer

This conservator type transformer has ONAN and oil-natural-air-force (ONAF) cooling modes and serves at the 33kV distribution level. The LV winding is a helical type winding with 94 turns. Each turn consists of 25 parallel conductors. The axial cooling channel is designed after the 12th conductor by inserting 5 mm cooling band, while the horizontal cooling channels are formed by the 3-mm axial spacer placed between turns or discs. The disc winding is divided into two sections i.e. S1(inner-side) and S2 (outer-side). The cooling configuration is the same as in section 2.1 where the oil enters from the bottom and leaves at the top of winding as illustrated in Figure 2. At rated condition, the LV winding carries load current of 1575A which equals to 2.22 A/mm^2 current density. Applying equations (5), (6) and (7) gives the total winding losses equals 16356 watts per phase.

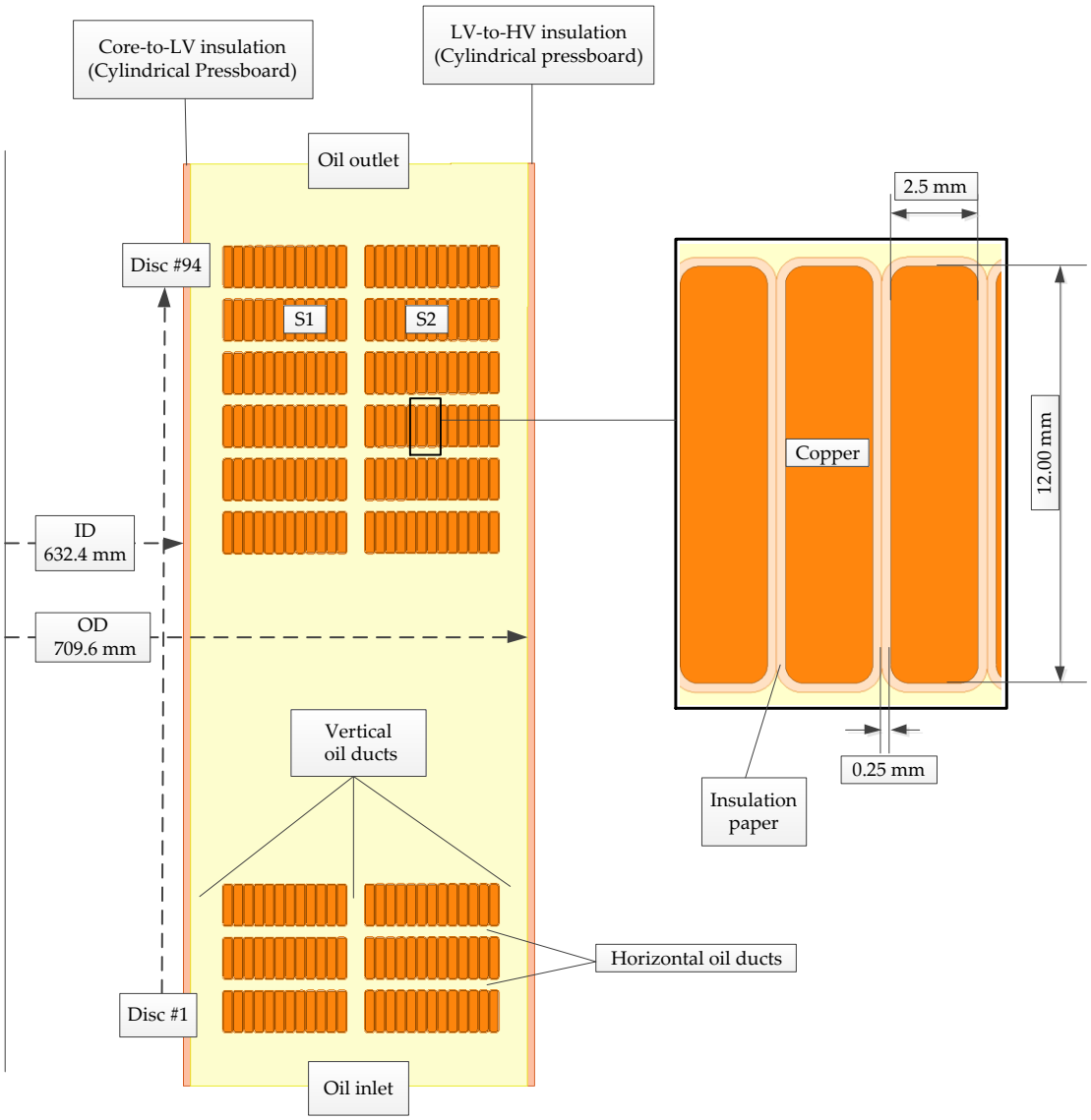

Figure 2. 2D axis-symmetry of 11kV low voltage winding with dimensions and a close-up view of detailed geometry and materials.

3. Methodology

The aim of this study is to have a fast and reliable calculation of transformer thermal distribution within windings by CFD. To achieve this, a simple 2D CFD winding model has been developed and analyzed. The SM is developed by considering one big conductor to represent all individual conductors as depicted in Figure 3(b) and Figure 3(f) for layer and disc windings respectively. This assumption is made due to the thermal conductivity of copper is far bigger than that of insulating paper (Kraft paper), as such the temperature gradient between conductor is negligible, thus the temperature difference across the insulation paper can be neglected [14].

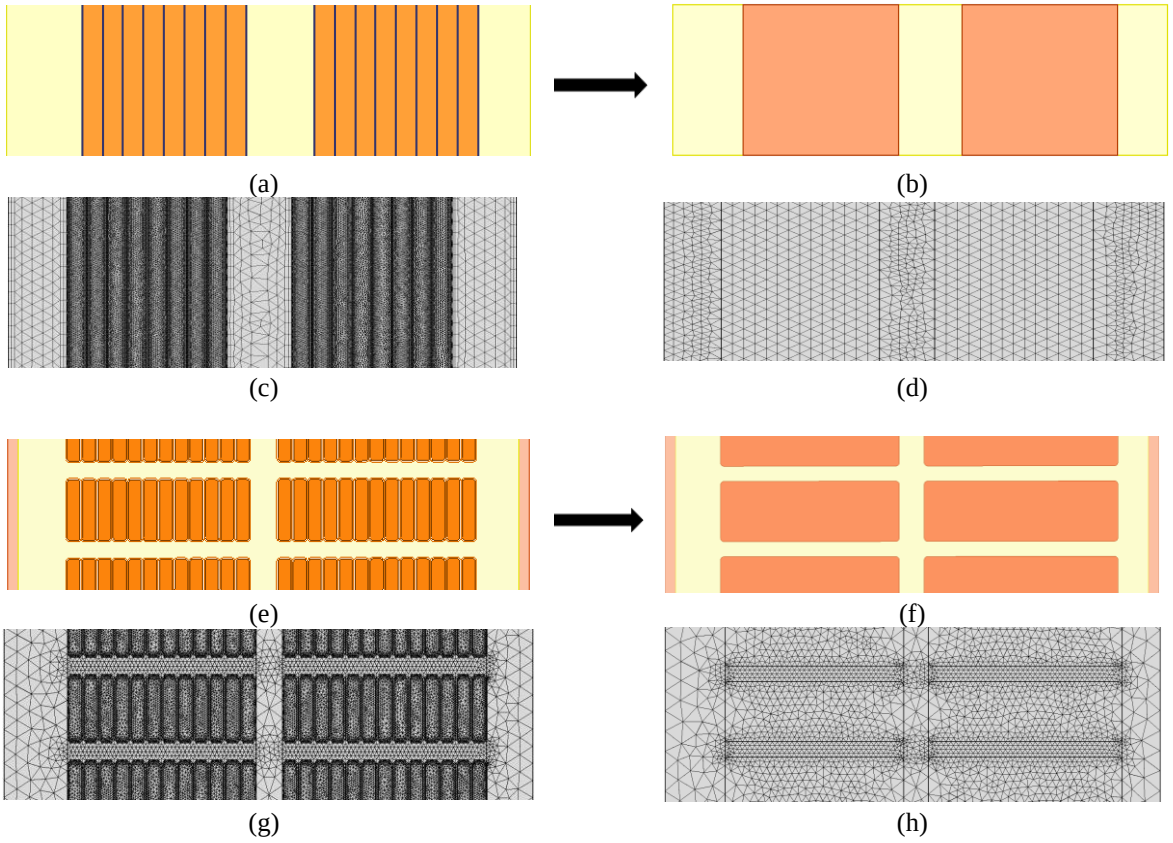

Figure 3. Illustration of simplification paper insulated copper conductor to one whole conductor (a) DM of 1000kVA LV winding (b) SM of 1000kVA LV winding (c) computational mesh for 1000kVA LV DM (d) computational mesh for 1000kVA LV SM (e) DM of 30MVA LV winding (f) SM of 30MVA LV winding (g) generated mesh for 30MVA LV DM (h) generated mesh for 30MVA LV SM.

From Figure 3(a) to Figure (c) and Figure 3(e) to Figure 3(f), it is noticed that the cross-sectional area of copper is increased by some factor. To ensure that the windings experience the same cooling effects, each disc must have the same surface contact area with the cooling oil. According to Newton's Law of Cooling [14]

$$Q_s = hA(T_s - T_\infty) \tag{8}$$

where Qs represents system heat source, h is the heat transfer coefficient; T_s and T_∞ are the temperatures on the surface and the surrounding respectively. A stands for the surface cooling area in contact with oil for one turn/disc can be obtained as the following;

$$A= AD\cdot\pi ID+2\cdot(RD\cdot l_{mean})+AD\cdot\pi OD \tag{9}$$

where AD and RD are the axial and radial dimensions of the conductor, while ID and OD are the inner and outer windings dimension respectively. The system heat source in the volumetric heat loss is given by

$$Q_s=\frac{P_{tot}}{V} \tag{10}$$

where P_{tot} is the total winding losses. V is the winding volume can be expressed as

$$V= AD\times RR\times l_{mean} \tag{11}$$

where RR is the winding radial dimension and l_{mean} represent the circumferential mean winding, which can be calculated as

$$l_{mean}= 2\pi\left(\frac{OD+ID}{4}\right). \tag{12}$$

3.1 Governing equations for oil flow and heat transfer model

To solve the oil flow problem, the compressible Navier-Stokes and continuity equations are applied while the general heat transfer equation is used to obtain the temperature distributions for both inside windings and moving oil. These equations are given as

$$\rho_f(\mathbf{u}\cdot\nabla)\mathbf{u} = \nabla\cdot\left[-p\mathbf{I}+\mu\left(\nabla\mathbf{u}+(\nabla\mathbf{u})\right)^T-\frac{2}{3}\mu(\nabla\cdot\mathbf{u})\mathbf{I}\right]+\rho_f g \tag{13}$$

$$\nabla\cdot\left(\rho_f\mathbf{u}\right) = 0 \tag{14}$$

$$\rho_f C_p\frac{\partial T}{\partial t}+\rho_f C_p\mathbf{u}\cdot\nabla T_f+\nabla\cdot(-k_f\nabla T_f) = Q_f \tag{15}$$

where **u** is the fluid velocity field, p denotes pressure, g is the gravitational acceleration and Q_f represents the heat in the fluid.

The buoyancy term is included on the right-hand side of equation (13) to justify the variation of buoyancy force due to changes in oil density caused by material thermal expansion. The first term of equation (15) can be neglected under steady-state study, in addition, the second term does not exist for solid material (copper winding and insulation paper).

The nature of oil flow inside the winding is characterized by three dimensionless parameters. The first parameter is the Reynolds number, Re which determines the flow either laminar, transition or turbulence. The flow is said to remain at laminar regime as long as the Reynolds number is below 2000 (classical value for fluid flow in the pipe). The second parameter is the Grashof number, Gr plays a significant role in natural convection that measures the ratio of the fluid buoyancy force to the viscous forces. The Prandtl number, Pr is the third parameter determines the relative effectiveness of momentum and energy transfer by diffusion in the velocity and thermal boundary layers. In addition, the ratio of Gr/Re^2 provides useful information on the flow regime, $Gr/Re^2 >> 1$ describes as natural convection while, $Gr/Re^2 <<1$ describes as forced convection[15]. These parameters can be found as

$$Re=\frac{\rho_f UL}{\mu} \tag{16}$$

$$Gr=\frac{g\beta(T_s-T_\infty)L^3}{\nu^2} \tag{17}$$

$$Pr=\frac{\nu}{\alpha} \tag{18}$$

where U is the velocity; L is the length of the system; β represents the coefficient of thermal expansion; ν and α are the kinematic viscosity and thermal diffusivity of fluid respectively

In this investigation, several assumptions were made during model development and computer simulations. The fluid flow was considered in a laminar flow regime due to low velocities of oil inside cooling channels and high value of dynamic viscosity. The 2D axisymmetric winding model was approached to reduce computational time. Cylindrical pressboards used to hold the formation of winding as well as to increase the electrical field strength between windings were considered adiabatic due to very low thermal conductivity approximately around 0.1W/mK, thus no heat enters or leaves the system i.e thermally insulated. The roughnous surfaces of winding insulation and cylindrical pressboard were ignored, hence no-slip wall was set. It is known that the eddy current losses are non-uniform for each disc or turn in the entire winding. Though, for practicality the winding losses were considered uniformly distributed between turns and discs.

The solid materials i.e. copper and insulation paper are homogenous and temperature independent. The buoyancy effects were measured as the product of oil density and gravitational acceleration. The constant ambient temperature and pressure were considered for this numerical simulation. On ONAN operation, the oil enters the winding only influenced by the buoyancy force inside the system, as such the boundary conditions for oil enters and exit the system were set as open boundaries. As can be seen from the expression (1) and (9), the buoyancy force decreases with the increase in temperature due to the low value of oil density.

4. Results and Discussions

Beneficial and meaningful information has been obtained in the numerical simulations of transformers with two different winding designs. It was well understood; the axially cooling design for medium power transformer was unable to predict or control the flow pattern of cooling oil horizontally.

4.1 1000kVA 11/0.433kV

Table 1. The average, gradient of winding and hot-spot temperatures between models.

Model	T_{ave} in ^oC	ΔT_{T-B} in K	$T_{Hot-Spot}$ in ^oC	T_{max} -T_{min} in K
DM	84.70	(89.94-76.92) = 13.02	90.44	(90.44-75.66) = 14.78
SM	85.90	(91.17-77.60) = 13.57	91.90	(91.90-77.55) = 14.35

Table 1 presents the results obtained from the numerical simulation of 1000kVA transformer. Overall, the results have shown no significant variation of temperature between DM and SM. The average winding temperature (T_{ave}) of SM was slightly higher by 1.42%. It was only 0.55K different in average winding temperature gradient (ΔT_{T-B}) between models. The hot-spot temperature ($T_{Hot-Spot}$) of DM was lower than SM by 1.46^{o}C while the maximum temperature difference (T_{max} -T_{min}) was differed by only 2.9%.

Surface velocity and temperature distribution plots on both DM and SM are presented in Figure 4 and Figure 6 respectively. The location of hot-spot temperature for both DM and SM are approximately in the area between 420mm and 430mm of winding height. The plotted graph in Figure 5 shows a comparison of mean oil velocity inside vertical

channels between detailed and simple models. The mean oil velocity is obtained and measured on the horizontal line drawn at respective winding height with the interval of 50 mm each. It can be seen, the middle oil channels (see DM_Ch2 and SM_Ch2) show the highest mean oil velocity for both models, while oil velocity in channel 1 and 2 (DM_Ch1, DM_Ch3, SM_Ch1 and SM_Ch3) are most likely have similar value and pattern. The changes in oil velocity are clearly visible between the oil entry region (winding bottom) and in the oil exit area (winding top). The average winding temperatures were plotted as shown in Figure 7 where the distribution shows insignificant variation between models. It is observed that the temperature linearly increases with the increasing of winding height. Though the average winding temperature stabilized at the end of the winding, that is between 350 mm 430 mm.

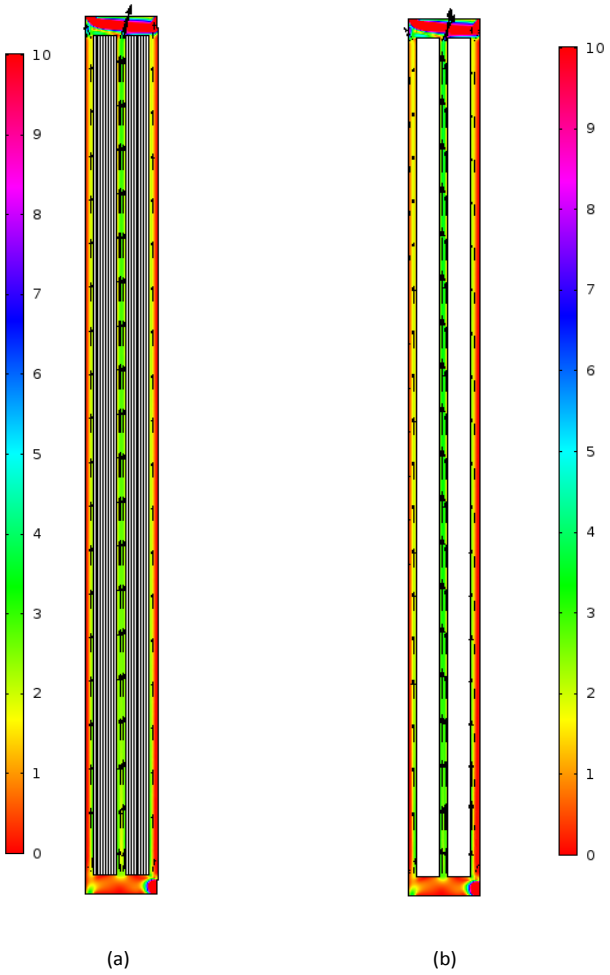

Figure 4. Oil velocity magnitude (mm/s) and arrow velocity field of (a) DM, (b) SM

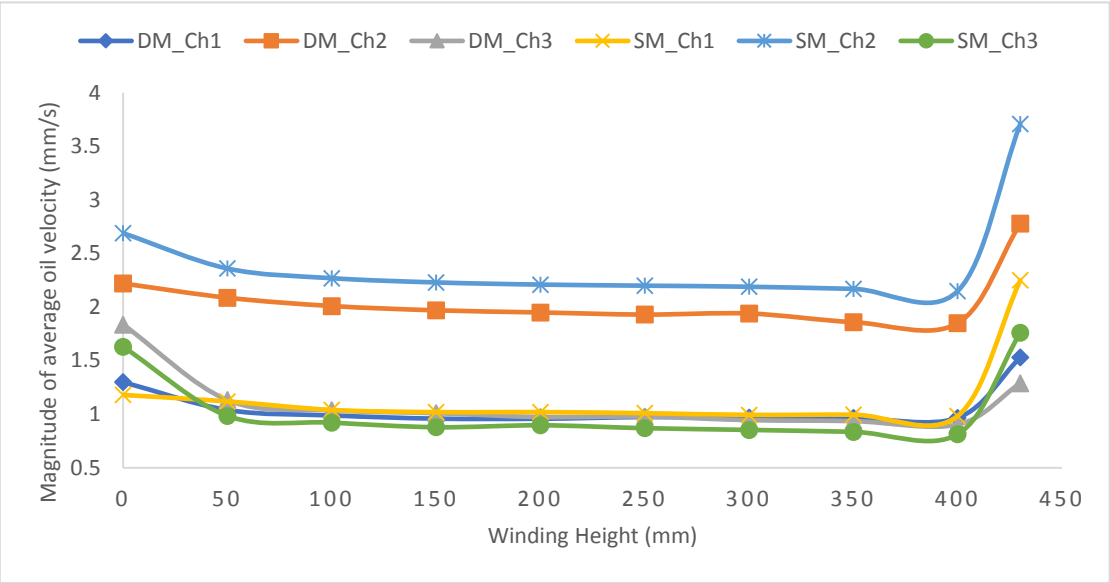

Figure 5. Average oil velocities inside channels between DM and SM corresponding to Figure 4 where Ch is the oil vertical channel.

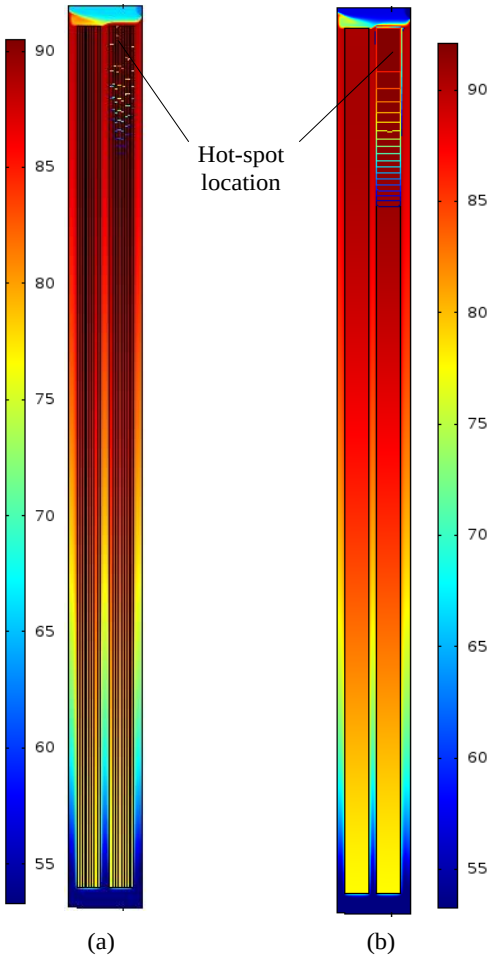

Figure 6. Thermal distribution (°C) plots on (a). DM, (b). SM

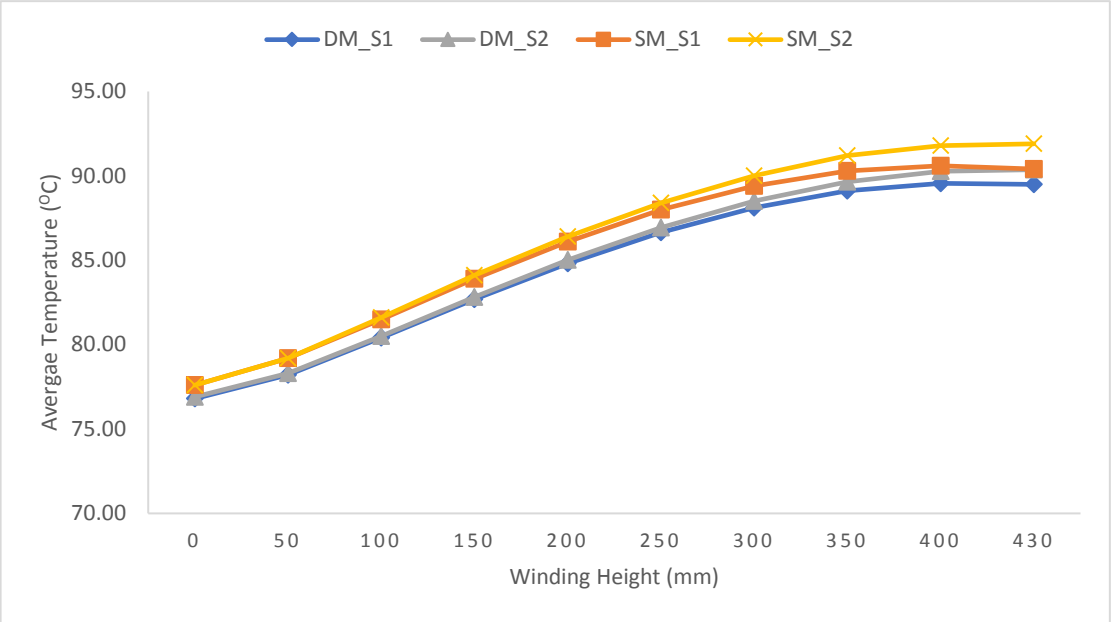

Figure 7. An average winding temperature in each section between models

The results of 3D plots between DM and SM are shown in Figure 8 where the thermal analysis was made as tabulated in Table 1.

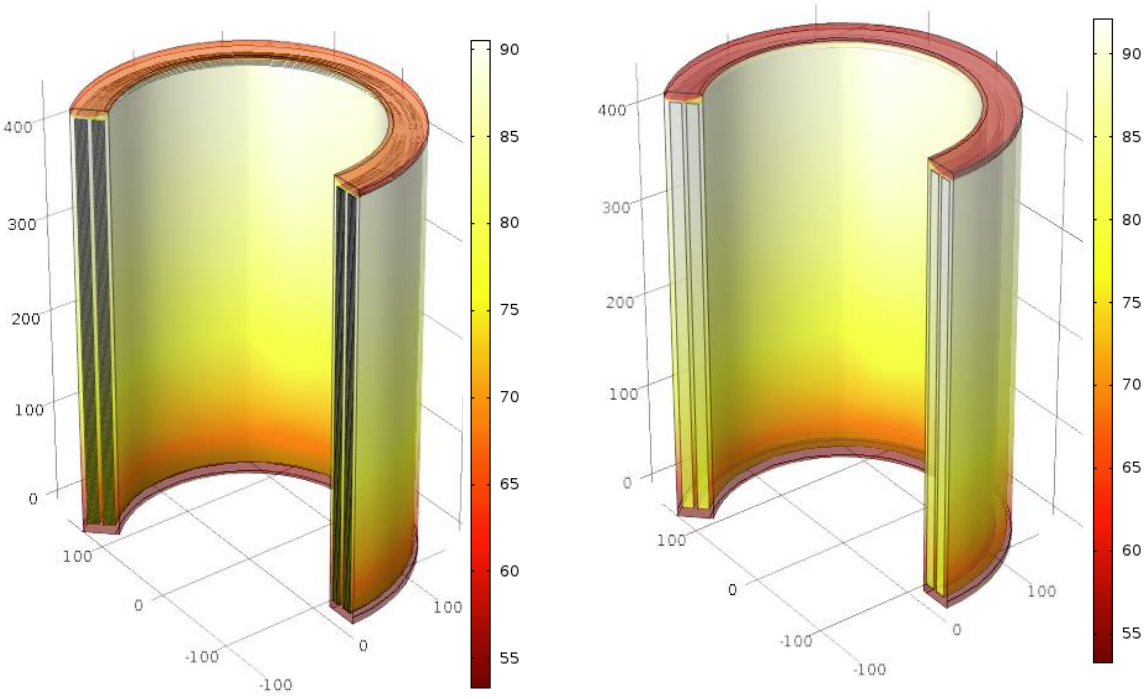

(a) (b)

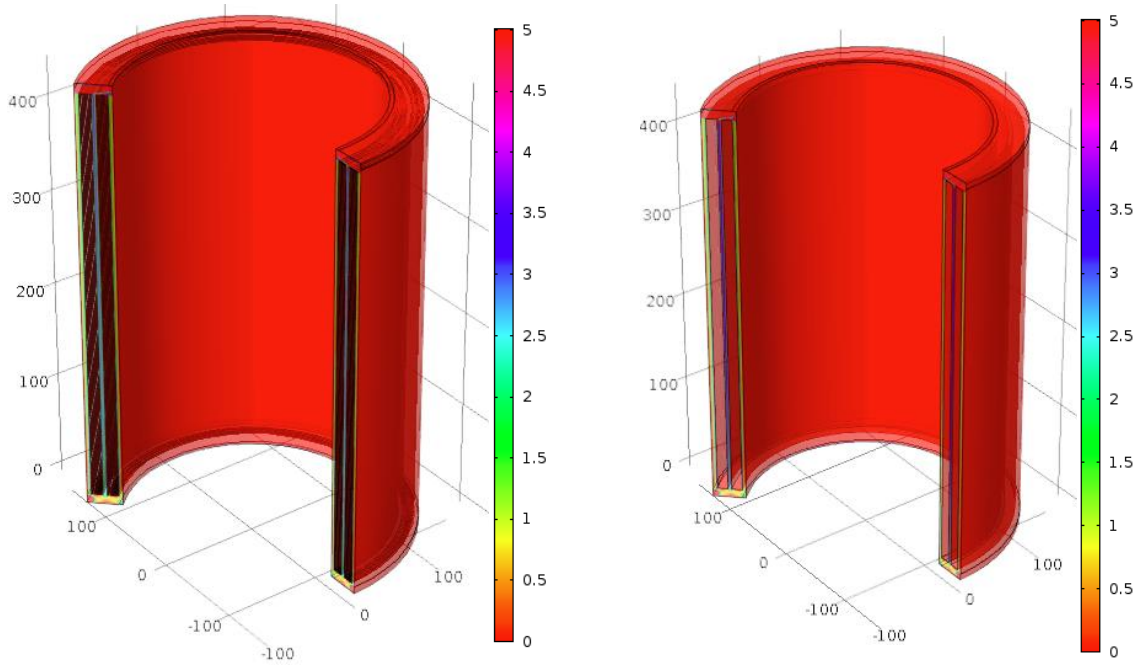

(c) (d)

Figure 8. (a) Temperature distribution of DM; (b) Temperature distribution of SM; (c) Magnitude of oil flow velocity of DM; (d) Magnitude of oil velocity flow of SM

4.2 30MVA 33/11kV

Table 2. Disc temperature data between models

Model	T_{ave} in ^oC	ΔT_{T-B} in K	$T_{Hot-Spot}$ in ^oC	T_{max}-T_{min} in K
DM	66.82	(64.72 - 62.69) = 2.03	84.20	(84.20 - 56.10) = 28.10
SM	64.84	(65.59 - 57.88) = 7.71	65.73	(65.73 -57.66) = 8.07

Table 2 presents the temperature data from the numerical simulation for 94 discs of 30MVA medium power transformer. As tabulated, the top to the bottom temperature gradient of winding (ΔT_{T-B}) of SM showed a big deviation as to the DM. It is almost 280% more than of that DM. On the other hand, the maximum temperature different (T_{max}-T_{min}) of SM is lower than DM by 20.03^{o}C. Besides that, the hot-spot temperature ($T_{Hot-Spot}$) of SM is very much lower than DM approximately by 18.47^{o}C. These foreseen results are due to the absence of insulation paper between the fluid and solid interface and as well as between conductors. Nevertheless, the average winding temperature (T_{ave}) exhibited insignificant variation between the models.

The plots of the magnitude oil flow velocity and temperature distributions are presented in Figure 9, which were resulted from the natural convection of oil. Figure 9(a) and 9(b) show the oil flow distribution of DM and SM respectively. Both exhibits quit similar maximum value of oil flow velocity that is around 51 mm/s. As depicted in Figure 9(c), the location of hot-spot temperature is on the disc number 93 (84.2°C) in S1 for DM, while for SM as shown in Figure 9 (d) is on the disc number 94 (65.73°C) in S2. There are also some high temperatures at the disc number 49 to 51 (approx.> 75°C) in S2 of DM. One of the reason was due to the least pressure difference developed in the relative junctions which leads to low oil flow region inside the respective horizontal ducts.

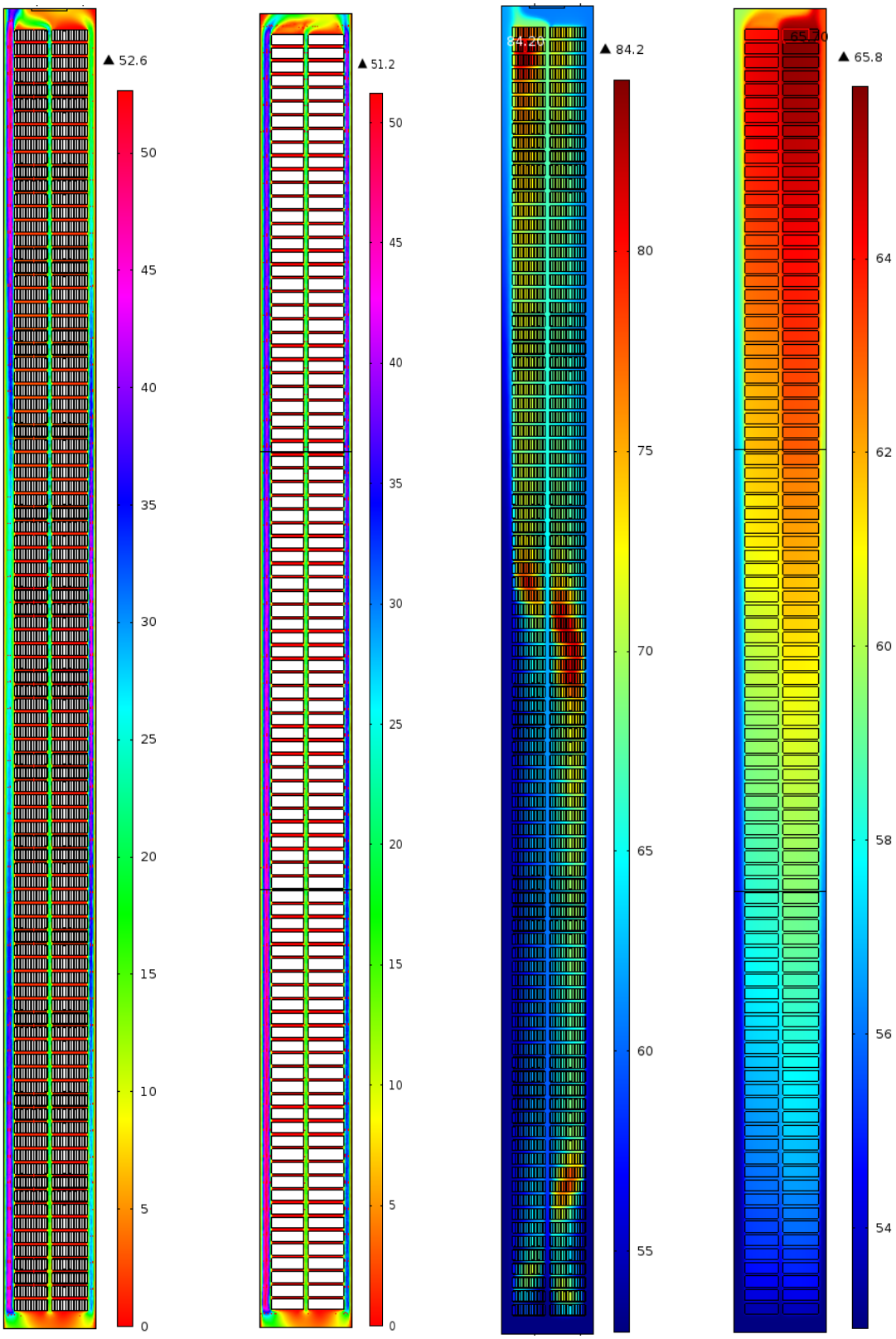

(a) (b) (c) (d)

Figure 9. 2D Distribution plots for (a) Magnitude oil flow velocity of DM in mm/s (b) Magnitude oil flow velocity of SM in mm/s (c) Temperature of DM in °C (d) Temperature of SM in °C

Figure 10 and Figure 11 are the plotted graphs to show comparisons between models for the magnitude of oil flow velocity and temperature distribution. The magnitude of oil velocity is calculated as an average magnitude of oil flow at the center of horizontal oil duct, while the temperature is calculated as an average disc temperature.

From Figure 10, for SM, the overall oil flow velocity of both SM_S1 and SM_S2 show uniform variation except inside the channel number 1 to number 24. Despite having a quite similar pattern, the oil flow of SM_S1 has the highest value of 1.5 mm/s inside the channel number 1. The highest oil flow value for S2 is 0.76 mm/s inside the channel number 33. For DM, the oil flow pattern is almost identical for both S1 and S2. The oil flow gradually rises until channel number 19 to 27 (in both S1 and S2) before it drops to almost zero at the channels number 53 for S1 and 50 for S2. Then, the oil flow rapidly increases to maximum values of 2.43 mm/s for S1 (channel 70) and 2.49 mm/s for S2 (channel 69). Inside the last oil channel i.e. number 93, the oil flow falls to 0.27 mm/s and 1.09 mm/s for both S1 and S2 respectively.

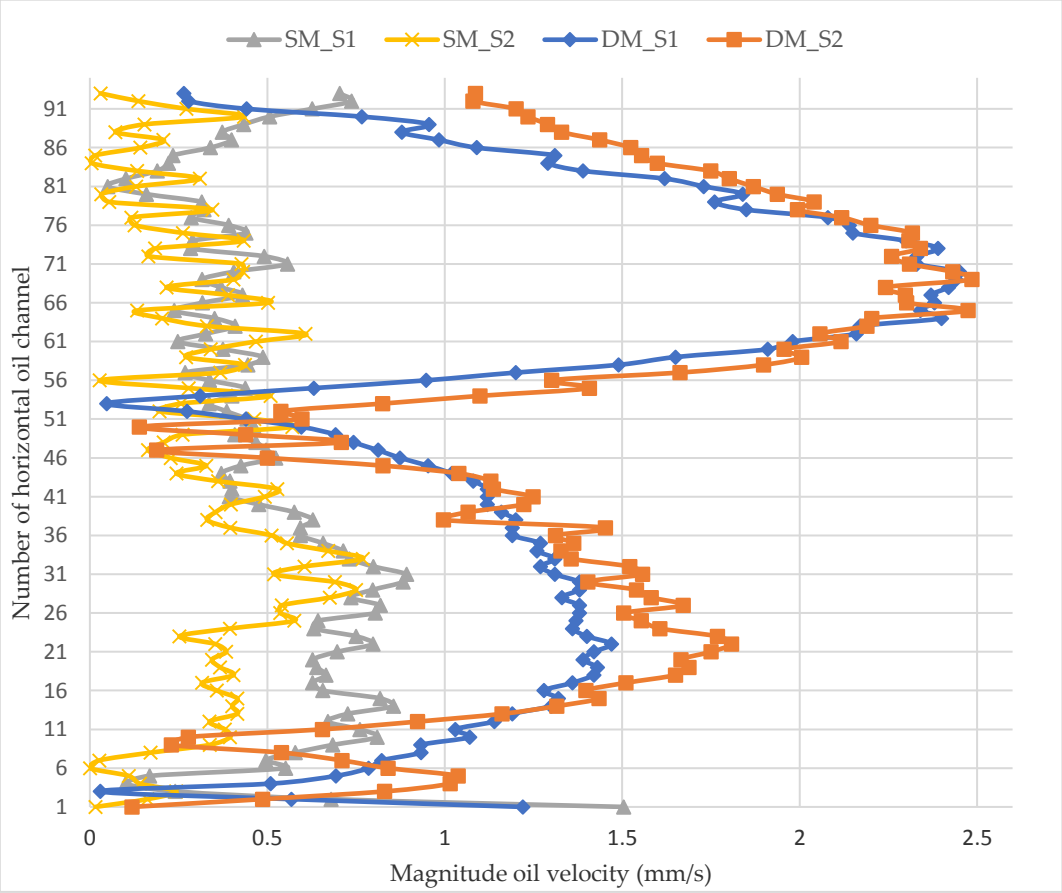

Figure 10. Comparison of magnitude oil velocity inside 3mm height horizontal oil cooling duct.

From Figure 11, each model shows quite a similar pattern of thermal distribution between discs. It is observed that the temperature of SM is linearly distributed with respects to the higher number of disc with the lowest value of 53.72°C (for both S1 and S2) at disc number 1 to 64.03°C (S1) and 65.73°C (S2) at disc number 94. For DM, due to unpredictable thermal distribution between discs, there are three hot-spot regions are developed. They are at discs number 10 (S2), 50 (S2) and 93 (S1) with an average value of 71.62°C, 76.54°C and 78.89°C respectively. The hottest temperature sits on the disc number 93 (S1) with the value of 84.2°C and the lowest temperature equals to 57.98°C at the disc number 1 of S2.

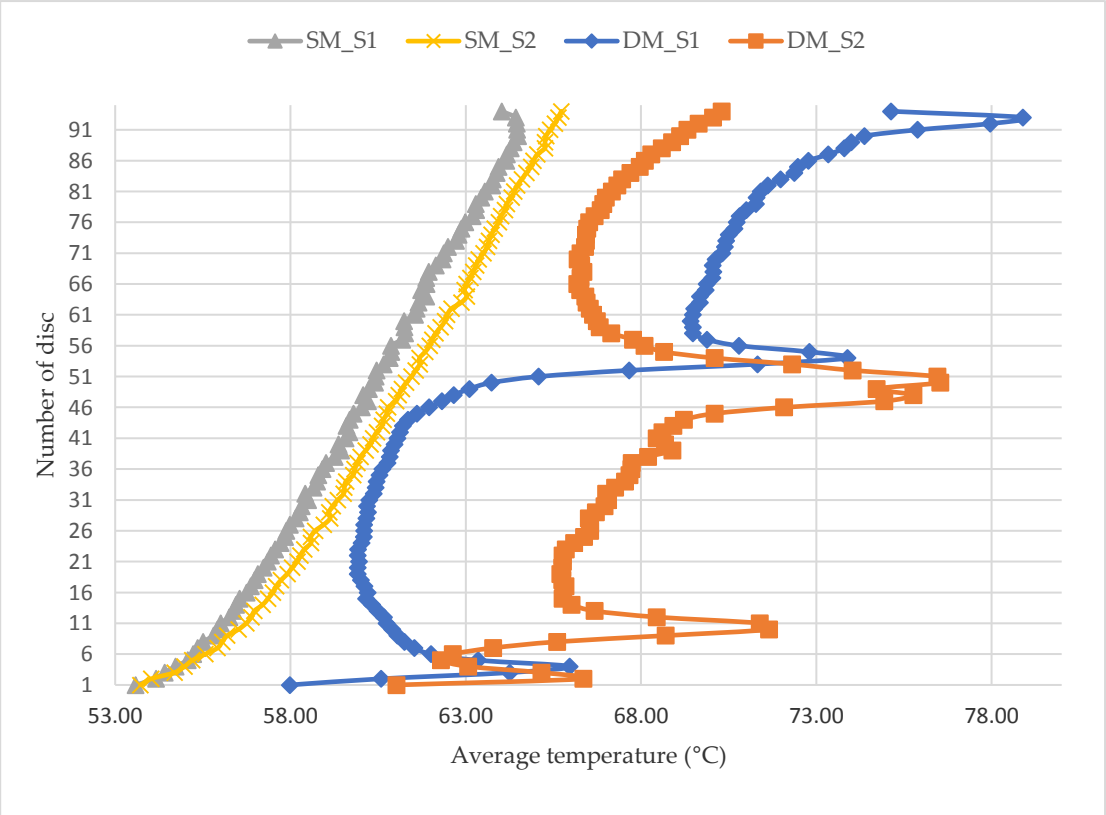

Figure 11. Comparison of average winding temperature between segments and models

Figure 12 shows the hot-spot location of DM at disc number 93. This hot-spot temperature lies in the lowest resultant radial oil flow region (black circle). In this region, as can be seen in Figure 13(b) the radial oil flow (range between +0.6 mm/s and -0.6 mm/s) components look very likely to have the same velocity in the opposite directions, consequently, oil-stagnant zone or eddies is formed. This scenario caused the oil inefficiently to transports the heat away, subsequently, the hottest region is developed. It is almost certain, in this case, the flow pattern of oil is straightforward related to the establishment of winding hot-spot temperature and its location as presented by [16].

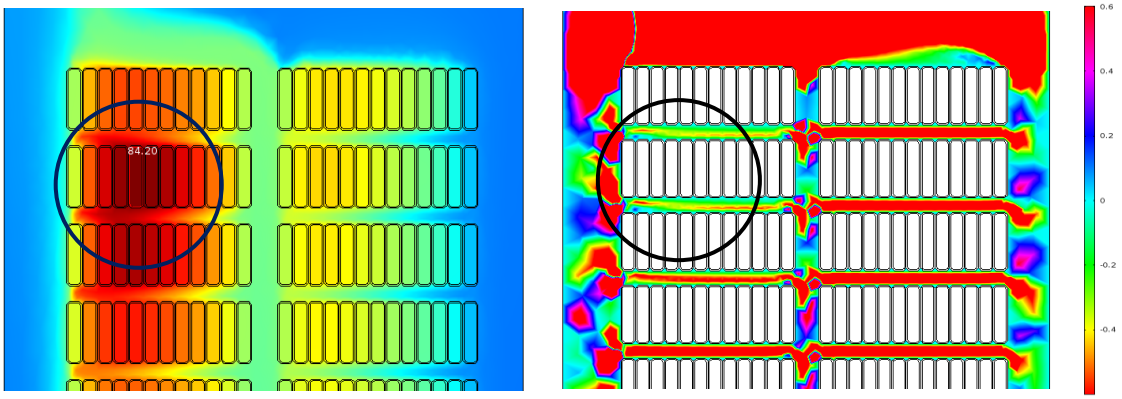

(a) (b)

Figure 12. Zoom in (a) the location of hot-spot temperature (b) radial component of the oil velocity field (mm/s).

The 3D plots for thermal and velocity distributions of DM and SM are shown in Figure 13 respectively. The thermal study as tabulated in Table 2.

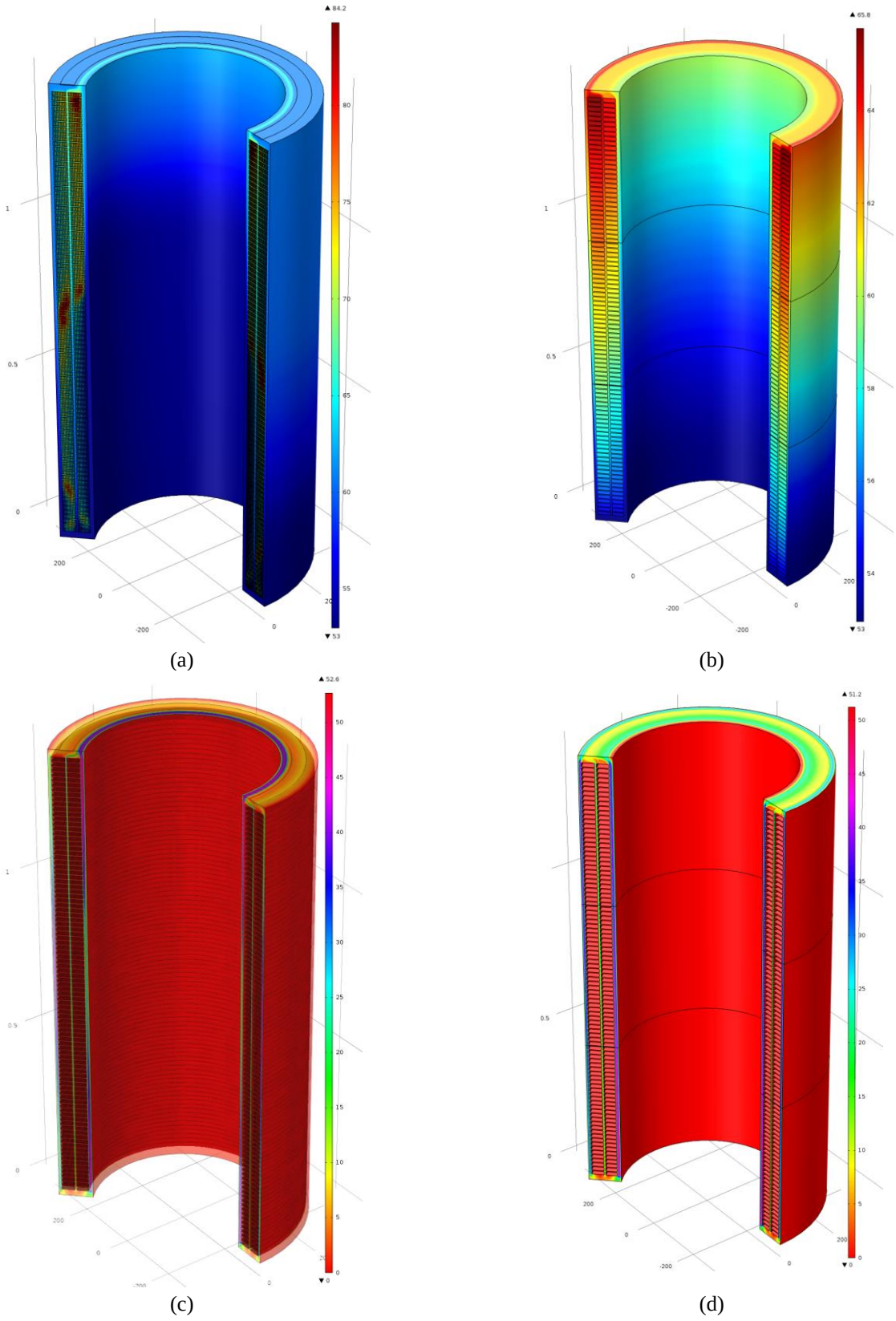

Figure 13. (a) Temperature distribution of DM; (b) Temperature distribution of SM; (c) Magnitude oil velocity of DM; (d) Magnitude oil velocity of SM.

5. Conclusions

In this study, the 2D approximation unable to model elements that influence the oil flow pattern such as axial spacers, top and bottom winding supports and other active-parts supporting structures. Thus, results obtained in 2D model possibly leading to improper analysis. Therefore, the full scale of the winding model is required if the objective is to obtain a very accurate prediction of hot-spot value and position. This CFD study employed sets of equations based on the theoretical fundamental of fluid flow and thermal distribution under natural convection phenomena. This work was designed to determine and analyze the thermal and liquid flow behaviors in layer/foil and disc windings. The establishment of fluid flow due to the buoyancy force is unpredictable for axial cooling duct winding design as in 30MVA transformer. This is because the flow direction is solely depending on buoyancy force due to gravitational pull and temperature dependent oil density. Obviously, the axially cooling design for power transformer is difficult to predict in terms of oil flow direction and hot-spot location. It is proven in this study there are three possibilities of hot-spot location in DM (disc no. 10, 50 and 93). For small distribution transformer with copper-foil winding shows no significant variation of thermal distribution between DM and SM. The difference in thermal distribution between DM and SM of 30MVA transformer winding models are very significant. It is clearly seen that simplification of winding models did not show good agreement with the DM in thermal distribution as well as on the oil flow pattern. In conclusion, the SM approximation is recommended for small distribution transformer but not for the bigger size of transformer i.e. power transformer.

Acknowledgments: The work for this article is supported by Universiti Teknikal Malaysia Melaka and Universiti Putra Malaysia.

References

[1] K. Dawood, M. A. Cinar, B. Alboyaci, and O. Sonmez, "Calculation of the leakage reactance in distribution transformers via numerical and analytical methods," *Journal of Electrical Systems*, vol. 15, no. 2, pp. 213–221, 2019.

[2] N. Ida, *Engineering Electromagnetics*, 1st ed. ; Springer-Verlag New York, Inc.: New York, USA, 2000.

[3] S. Taheri, A. Gholami, I. Fofana, and H. Taheri, "Modeling and simulation of transformer loading capability and hot spot temperature under harmonic conditions," *Electric Power Systems Research*, vol. 86, pp. 68–75, 2012.

[4] P. S. Moses and M. A. S. Masoum, "Three-phase asymmetric transformer aging considering voltage-current harmonic interactions, unbalanced nonlinear loading, magnetic couplings, and hysteresis," *IEEE Transactions on Energy Conversion*, vol. 27, no. 2, pp. 318–327, 2012.

[5] Z. Radakovic, M. Sorgic, W. Van Der Veken, and G. Claessens, "Ratings of oil power transformer in different cooling modes," *IEEE Transactions on Power Delivery*, vol. 27, no. 2, pp. 618–625, 2012.

[6] IEC 60076-7, "Power Transformer-Part 7: Loading guide for Oil-Immersed Power Transformer," *International Electrotechnical Commission*, 2005.

[7] H. M. . Campelo, X. M. Lopez-Fernandez, P. Picher, and F. Torriano, "Advanced Thermal Modelling Techniques in Power Transformers . Review and Case Studies," *Advanced Research Workshop on transformers*, no. October, pp. 1–17, 2013.

[8] H. M. . Campelo, R. C. Lopes, J. C. B. Lopes, C. M. Fonte, and M. M. Dias, "Network modelling applied to CORE power transformers and validation with CFD simulations," in *International Colloquium Transformer Research and Asset Management Dubrovnik, Croatia, May 16-18,2012*, 2012, pp. 1–16.

[9] R. Gong, J. Ruan, J. Chen, Y. Quan, J. Wang, and S. Jin, "A 3-D coupled magneto-fluid-thermal analysis of a 220 kV three-phase three-limb transformer under DC bias," *Energies*, vol. 10, no. 4, 2017.

[10] H. M. R. Campelo, M. A. Quintela, F. Torriano, P. Labbe, and P. Picher, "Numerical thermofluid analysis of a power transformer disc-type winding," *34th Electrical Insulation Conference, EIC 2016*, no. June, pp. 362–365, 2016.

[11] S. B. Paramane, W. Van Der Veken, A. Sharma, and J. Coddé, "Effects of oil leakage on thermal hydraulic

characteristics and performance of a disc-type transformer winding," *Applied Thermal Engineering*, vol. 98, pp. 1130–1139, 2016.

[12] W. Guan *et al.*, "Finite element modeling of heat transfer in a nanofluid filled transformer," *IEEE Transactions on Magnetics*, vol. 50, no. 2, pp. 2–5, 2014.

[13] W. Wu *et al.*, "Computational fluid dynamics calibration for network modelling of transformer cooling oil flows – Part I heat transfer in oil ducts," *IET Electric Power Applications*, vol. 6, no. January 2011, p. 28, 2012.

[14] F. P. Incropera, D. P. DeWitt, T. L. Bergman, and A. S. Lavine, *Fundamentals of Heat and Mass Transfer*. 2007.

[15] F. Torriano, M. Chaaban, and P. Picher, "Numerical study of parameters affecting the temperature distribution in a disc-type transformer winding," *Applied Thermal Engineering*, vol. 30, no. 14–15, pp. 2034–2044, 2010.

[16] A. Gustafsson, Y. Jiao, A. B. B. Ab, and P. Grids, "Transformer Winding Oil Flow Rate & Hot Spot Temperature : a Straightforward Relationship ?," in *The 21st Conference of The Electric Power Supply Industry*, 2016.